

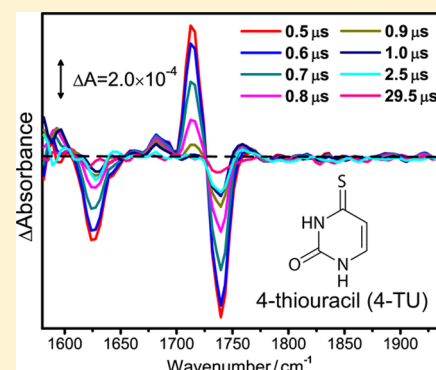
Photophysical and Photochemical Properties of 4-Thiouracil: Time-Resolved IR Spectroscopy and DFT Studies

Xiaoran Zou, Xiaojuan Dai, Kunhui Liu, Hongmei Zhao, Di Song, and Hongmei Su*

State Key Laboratory of Molecular Reaction Dynamics, Beijing National Laboratory for Molecular Sciences (BNLMS), Institute of Chemistry, Chinese Academy of Sciences, Beijing 100190, China

Supporting Information

ABSTRACT: Intensified research interests are posed with the thionucleobase 4-thiouracil (4-TU), due to its important biological function as site-specific photoprobe to detect RNA structures and nucleic acid–nucleic acid contacts. By means of time-resolved IR spectroscopy and density functional theory (DFT) studies, we have examined the unique photophysical and photochemical properties of 4-TU. It is shown that 4-TU absorbs UVA light and results in the triplet formation with a high quantum yield (0.9). Under N₂-saturated anaerobic conditions, the reactive triplet undergoes mainly cross-linking, leading to the (5–4)/(6–4) pyrimidine–pyrimidone product. In the presence of O₂ under aerobic conditions, the triplet 4-TU acts as an energy donor to produce singlet oxygen ¹O₂ by triplet–triplet energy transfer. The highly reactive oxygen species ¹O₂ then reacts readily with 4-TU, leading to the products of uracil (U) with a yield of 0.2 and uracil-6-sulfonate (U^SO₃) that is fluorescent at ~390 nm. The product formation pathways and product distribution are well rationalized by the joint B3LYP/6-311+G(d,p) calculations. From dynamics and mechanistic point of views, these results enable a further understanding for 4-TU acting as reactive precursors for photochemical reactions relevant to ¹O₂, which has profound implications for photo cross-linking, DNA photodamage, as well as photodynamic therapy studies.

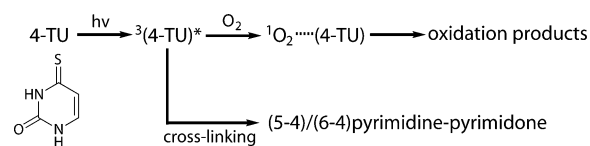


1. INTRODUCTION

Nucleic acid bases are the dominant chromophores accounting for the photochemical and photophysical properties of the nucleic acids upon irradiation below 300 nm.¹ UV absorption of nucleic bases initially generates singlet excited states which relax rapidly to the ground electronic state primarily via ultrafast internal conversion due to the existence of conical intersections.^{2–5} Recently, the role of long-lived (>10 ps) dark state ¹nπ* in DNA systems was highlighted due to its significance in solution-phase dynamics and the photostability of nucleic acids.^{6,7} By means of transient absorption spectroscopy,^{8–10} fluorescence up-conversion^{11–13} and the ultrafast time-resolved infrared (TRIR) measurements,¹⁴ the excited state dynamics and lifetimes of nucleosides, nucleotides, and isolated bases in solution have been measured to be in the picosecond or subpicosecond time range. Consequently, the nucleic bases are considered to be stable and refractory to photochemical pathways that lead to damage of DNA/RNA. Besides the regular bases, there are some base analogues identified as minor bases in tRNA,^{15–17} in particular, the thionucleobases. The substitution of oxygen atom by the sulfur atom makes the ultraviolet absorption of thionucleobases red-shifted and absorb UVA light (>300 nm), resulting in unusual photophysical and photochemical properties.^{18–20} Due to their biological effects and widespread application in pharmacology^{21–23} and molecular biology,^{18,24} research interests have been intensified for those thionucleobases in recent years.

Among the thionucleobases, 4-thiouracil (4-TU, shown in Scheme 1) is known to possess cytostatic properties and is

Scheme 1. Molecular Structure of 4-TU and Possible Photochemical Reactions



usually used as biological photoprobes as well as transcriptional regulation agent, based on its photo cross-linking reaction with other nucleic acids.^{18,25,26} With a strong UVA absorption maximum at ~330 nm, 4-TU can act as a site-specific optical probe for cross-linking studies.¹⁸ The photo cross-linking occurs between the C=S bond of the triplet state of 4-TU and the C5=C6 bond of the ground state of pyrimidine bases, leading to the (5–4) or (6–4) pyrimidine–pyrimidone photoproduct (Scheme 1).^{19,20} David S. Kligler and his co-workers studied photophysical properties of 4-thiouridine, 1,3-dimethyl-4-thiouracil, and uracil in aqueous solution by laser flash photolysis and indicated that the intersystem crossing

Received: February 16, 2014

Revised: May 4, 2014

Published: May 12, 2014

yield of 4-thiouridine is 0.9 ± 0.1 , which is much higher than uracil, its parent nucleic acid.²⁰ Such a high triplet quantum yield can be explained by the multiconfigurational self-consistent field (MCSCF) and time-dependent density functional theory (TD-DFT) calculations, which indicated that the dark $n\pi^*$ state of 4-TU can serve as a doorway state leading to the efficient intersystem crossing to the lowest triplet $\pi\pi^*$ because the energy gap between the two states is minor.²⁷

In addition to its high quantum yield of triplet state, interesting photochemical liability to generate singlet oxygen (1O_2) by photosensitization was suggested (Scheme 1). For 4-thiouridine under UVA irradiation, the quantum yield of the photosensitized formation of 1O_2 was determined to be 0.5 and 0.2 in acetonitrile and water, respectively.²⁸ The quenching rate constant of 4-TU triplet state by oxygen is $4 \times 10^9 \text{ M}^{-1} \text{ s}^{-1}$.¹⁸ As a type of reactive oxygen species (ROS), 1O_2 is highly reactive toward nucleobases, including the 4-TU itself. In fact, it was found that UVA irradiation of the dilute solution of 4-thiouridine can form uridine in aerobic conditions.¹⁸ The transformation of 4-thiouridine to uridine may be due to the reaction between 4-thiouridine and 1O_2 generated by the energy transfer from triplet state of 4-thiouridine, which is similar to another thionucleobase, 6-thioguanine.^{29,30} For 4-TU under irradiation in aerobic conditions, the triplet–triplet energy transfer to form 1O_2 may strongly compete with the photo-cross-linking of the triplet state of 4-TU with other bases (Scheme 1), influencing the efficiency of 4-TU as the biological photoprobe. Therefore, understanding of the photochemical reactions involving 1O_2 in aerobic conditions is certainly desirable.

In this paper, we perform joint experimental and theoretical investigation to examine the unique photochemical and photophysical properties of 4-TU at both aerobic and anaerobic conditions. Experimentally, Time-resolved infrared (TRIR) absorption spectroscopy and fluorescence spectroscopy have been applied to monitor the triplet excited state formation upon 355 nm excitation and its subsequent photochemical reactions in real-time. In N_2 -saturated anaerobic conditions, triplet state of 4-TU is clearly observed with a lifetime of $0.23 \pm 0.02 \mu\text{s}$ and the formation of 4-TU cross-linking product (5–4)/(6–4) pyrimidine-pyrimidone can also be detected. In O_2 -saturated aerobic conditions, the triplet 4-TU is quenched efficiently, leading to 1O_2 through photosensitization. 1O_2 then reacts readily with 4-TU and the oxidation products of uracil-6-sulfonate (U^{SO_3}) and uracil (U) are observed. Using density functional theory, we have explored the energetics and intermediates for 4-TU reacting with 1O_2 . The calculated mechanisms can properly rationalize the observed products and their distributions. From dynamics and mechanistic point of views, these results enable a further understanding for 4-TU acting as reactive precursors for photochemical reactions relevant to 1O_2 , which has profound implications for photo cross-linking, DNA photodamage, as well as photodynamic therapy studies.

2. EXPERIMENTAL AND COMPUTATIONAL METHODS

2.1. Experiments. TR-FTIR Experiments. The transients and photoproduct formation dynamics is monitored by step-scan, time-resolved Fourier transform infrared (TR-FTIR) absorption spectroscopy.^{31,32} Step-scan FTIR spectrometers are commercially available but require significant modification for applications on flash photolysis TRIR study. The TR-FTIR instrument comprises a Nicolet Nexus 870 step-scan FTIR

spectrometer, a Continuum Surelite II Nd YAG laser, a pulse generator (Stanford Research DG535) to initiate the laser pulse and achieve synchronization of the laser with data collection, two digitizers (internal 100 kHz 16-bit digitizer and external 100 MHz 14-bit GAGE CS14100 digitizer) which offer fast time resolution and a wide dynamic range as needed, and a personal computer to control the whole experiment. The detector used in this work is a photovoltaic MCT detector (0.5 mm) equipped with a fast internal preamplifier (50 MHz).

There are two outputs from the detector: output DC, corresponding to the value of the static interferogram; and output AC, corresponding to the time-resolved change of the interferogram. The AC signal was then amplified by an external preamplifier (Stanford Research, SR560). The differential absorbance spectra are calculated based on the equation:

$$\Delta A = A_{AC+DC} - A_{DC} = -\log_{10}(1 + \Delta I_{AC}/I_{DC})$$

where I_{DC} and ΔI_{AC} are the single-beam intensity spectra corresponding to static (DC) and dynamic (AC) channels. ΔI_{AC} is calibrated before being used in equation because different gain is applied to the AC channel.^{31,32}

The third harmonic of Nd: YAG laser (355 nm) operating at 10 Hz repetition rate were used in the experiments. The laser excitation beam was directed through an iris aperture (3 mm in diameter) and then overlapped with the infrared beam in the sample cell within the sample compartment of the FTIR spectrometer. The laser beam energy after the aperture was 3 mJ per pulse. A Harrick flowing solution cell with 2 mm-thick CaF_2 windows (path-length: 500 μm) was used for the measurements. The closed flowing system is driven by a peristaltic pump (ColeParmer Masterflex) to refresh the sample before every laser pulse.

The UV and Fluorescence Spectrum Experiments. The UV absorption spectra were taken on a Shimadzu UV1601 spectrophotometer. Fluorescence excitation and emission spectra were obtained using a HITACHI f-4600 fluorescence spectrophotometer.

Materials. 4-Thiouracil (Sigma-Aldrich, 98%) and $KMnO_4$ (Sinopharm Chemical Reagent Co., Ltd., $\geq 99.5\%$) were used as received. Solvent of HPLC grade of acetonitrile was used to obtain desirable spectroscopic windows for the TR-FTIR measurements. Ultrapure water obtained by Millipore filtration and phosphate buffer (pH = 7.0) were also used as solvent. The solutions were saturated with N_2 or O_2 depending on different experimental conditions.

2.2. Computational Methods. The geometries and harmonic vibrational frequencies of the reactants, products, intermediates, and transition states were calculated using the hybrid density functional theory (B3LYP) with the standard basis sets of 6-311+G(d,p),^{33,34} which is usually a sufficient and affordable computational method for the current system with a commensurate size of two 4-TU molecules. The harmonic frequency analysis was performed to identify the stationary point as either local minima (reactant, products, and intermediates) or first-order saddle points (transition states) and to extract zero-point vibrational energy corrections. Connections of the transition states between two local minima have been confirmed by intrinsic reaction coordinate (IRC) calculations at the same level.³⁵ Bulk solvation effects were simulated by using the polarizable continuum model (PCM).³⁶

Geometry optimizations of ground state 4-TU, 4-TU triplet state, photo-cross-linking product, and intermediates were performed at the B3LYP/6-311+G(d,p) level of theory with

the PCM to simulate bulk solvation effects. All stationary points were confirmed to be energy minima using vibrational frequency calculations (B3LYP/6-311+G(d,p)), which confirmed that all of the computed vibrational frequencies were real (i.e., no imaginary vibrational frequencies). Using the ground state stationary structures, the vertical electronic excitation were calculated with time-dependent DFT at the B3LYP/6-311+G(d,p) level and WB97XD/6-311+G(d,p) level. The TD-DFT method with the WB97XD functional,³⁷ the B3LYP functional and the 6-311+G(d,p) basis sets were applied to fully optimize the excited-state equilibrium structures, from which the emission wavelengths and oscillator strength were computed. All the calculations were carried out using the Gaussian 09 program package.³⁸

3. RESULTS AND DISCUSSION

3.1. Electronic Configuration of the Excited States of 4-TU. Steady-state absorption properties for 4-TU are first characterized. Figure 1 shows the UV–vis absorption spectra of

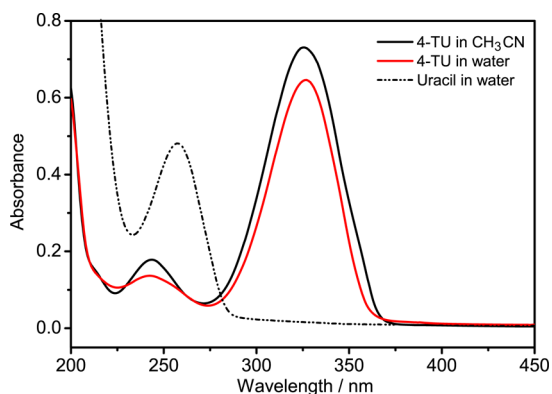


Figure 1. UV–vis absorption spectra of 4-thiouracil (red solid line), uracil (dash dot line) in aqueous solution and 4-thiouracil in acetonitrile (black solid line).

4-TU in CH₃CN and in aqueous solution. For comparison, the spectrum of the corresponding normal nucleobase uracil is also shown. Unlike uracil, 4-TU absorbs UVA light strongly, exhibiting a strong band with a maximum at ~327 nm. According to its large molar absorption coefficient ($\epsilon = 19380 \text{ M}^{-1} \text{ cm}^{-1}$), the 327 nm band should be attributed to a π, π^* transition, which is in agreement with the assignment for 4-thiouridine in CCl₄.³⁹ Wavelengths of absorption peaks and molar absorption coefficients for 4-TU are summarized in Table 1. To further ascribe its electronic configurations, vertical excitation energies and oscillator strength of the excited singlet states were calculated with the method of TD-DFT and the calculated results are also listed in Table 1.

The n, π^* transition is calculated to lie significantly below the lowest π, π^* transition. Due to its quite low oscillator strength (<0.0001), the n, π^* transition belongs to a dark state that can not be observed in the absorption spectrum. Therefore, the intense absorption band at 327 nm can be assigned to the transition to the second lowest excited singlet S_2 state which is of a π, π^* character with a strong oscillator strength (0.30), lying above the lowest excited singlet (S_1) state of the dark n, π^* state. In addition to this UVA band, there is also a weaker UVB absorption band at 240 nm, corresponding to another π, π^* transition to S_6 state. As shown in Table 1, the steady-state absorption data are in good agreement with the vertical

Table 1. Ground-State Absorption Spectrum, Calculated Vertical Excitation Energies (E_{calc}), and Oscillator Strengths (f_{calc}) of the Excited Singlet States of 4-TU

transitions from S_0	$\lambda_{\text{max}}^a / \text{nm} (\text{cm}^{-1})$	$\epsilon^b / \text{M}^{-1} \text{cm}^{-1}$	$E_{\text{calc}}^{c,d} / \text{nm} (\text{cm}^{-1})$	f_{calc}^c
$S_1 n, \pi^*$			473(21126)	0.0000
$S_2 \pi, \pi^*$	327(30581)	19 380	314(31873)	0.2989
$S_3 n, \pi^*$			286(34948)	0.0003
$S_4 \pi, \pi^*$			274(36521)	0.0078
$S_5 n, \sigma^*$			262(38142)	0.0089
$S_6 \pi, \pi^*$	242(41322)	4139	257(38887)	0.1324

^aThe wavelengths of maximum absorption. ^bThe molar absorption coefficient at the absorption peak. ^cCalculated by the TD-DFT method for the molecular configuration optimized in the S_0 state at the B3LYP/6-311+G(d,p) level. ^dThe values were scaled by 0.94.

excitation energies and oscillator strengths obtained from TD-DFT calculations.

Two tautomers may exist for the thionucleobases, thione or thiol form. It has been shown that 4-thiouracil derivatives exist exclusively in the (C-2)-keto-(C-4)-thione tautomeric structure in vapor, solid state as well as in aqueous, organic solvents.^{20,40,41} Indeed, the location of both absorption maxima, the spectral width and the profile, as well as the intensity of the absorption bands of 4-TU observed here are identical to those of 1, 3-dimethyl-4-thiouracil (DMTU),⁴² whose (C-2)-keto-(C-4)-thione tautomeric structure is fixed by methyl groups, demonstrating further that 4-TU adopts solely the thione structure in solution.

3.2. Anaerobic Conditions: Triplet and Its Photochemistry Characterization with TR-FTIR Absorption Spectroscopy. Upon UVA excitation of 4-TU to its S_2 state, intersystem crossing can lead to efficient triplet state population, which is an origin of the unique photophysical and photochemical behavior of this molecule. TR-FTIR measurements were performed to obtain the detailed (spectral and kinetic) information for the triplet state of 4-TU. Figure 2b shows the transient IR absorption spectrum of 4-TU (1.0 mM, saturated with N₂ before and during the experiments) obtained after the nanosecond 355 nm laser irradiation. Immediately after UV excitation, two intense bleaching bands at 1623 and 1735 cm^{-1} were observed, which should be ascribed to the depletion of ground state molecules. The steady-state IR absorption spectrum for the ground state 4-TU (Figure 2a) reveals these two identical bands, confirming the assignment. To aid the assignment of the IR bands observed in the FTIR experiment, IR frequencies and intensities were calculated at the B3LYP/6-311+G(d,p) level for the relevant species (Table 2) that may be formed in these reactions. Bulk solvation effects were simulated by using the PCM model. The calculated IR frequencies of 1637 (C5=C6 stretching mode) and 1744 cm^{-1} (C2=O stretching mode) for the ground state 4-TU in acetonitrile are in agreement with the observed peak wavelength at 1623 and 1735 cm^{-1} in the steady-state IR absorption spectrum (Figure 2a). The current level of calculation can predict reliable IR frequencies for spectral assignment purpose.

The ground state bleaching bands are accompanied by the formation of a positive band at 1712 cm^{-1} in the transient IR spectra. For the characteristic bands at 1712 cm^{-1} , kinetic traces are also shown in the inset of Figure 2b, together with that for the ground state bleaching band at 1735 cm^{-1} . The positive band decay is simultaneous with the ground state recovery, with

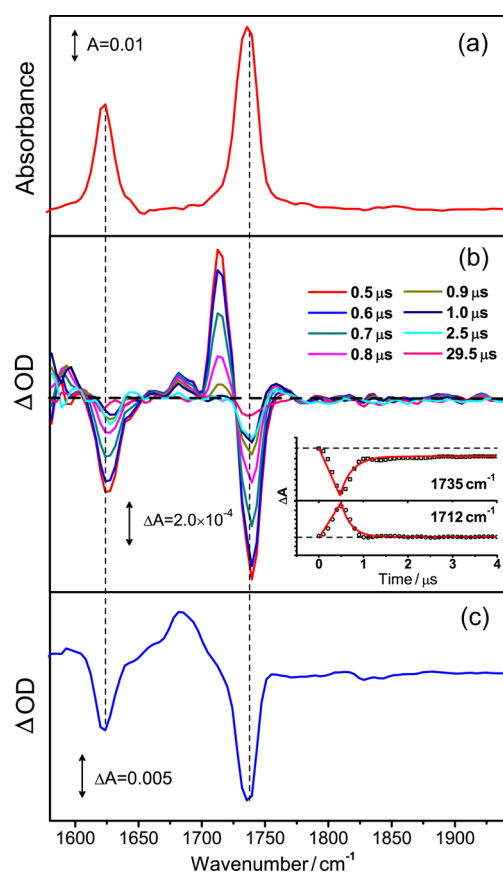
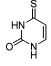
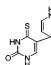
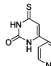
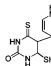
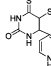
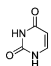


Figure 2. (a) Steady-state IR absorption spectrum of 1.0 mM solution of 4-TU in acetonitrile. (b) Infrared transient absorption (TR-FTIR) spectra of 1.0 mM solution of 4-TU in acetonitrile saturated with N_2 following 355 nm laser irradiation. Inset: Kinetic traces for triplet 4-TU formation at 1712 cm^{-1} and ground state 4-TU bleach at 1735 cm^{-1} . (c) Steady-state IR difference spectrum of 4-TU (1.0 mM) in acetonitrile saturated with N_2 after 1 min of 355 nm laser irradiation. All the spectra were collected with a spectral resolution of 8 cm^{-1} .

a lifetime of $0.23 \pm 0.02\ \mu\text{s}$ obtained from single exponential fitting. Upon oxygenation, almost all of the transient features disappear, which indicates that the positive band as well as most of the ground state bleaches is ascribed to the triplet formation. Further evidence is provided by our calculations (Table 2), predicting a $C=O$ vibration at 1712 cm^{-1} for the triplet state of 4-TU, which coincides with the observed spectral position. Thus, the transient 1712 cm^{-1} band is assigned to the lowest triplet state of 4-TU.

From the amplitude of the triplet state band at 1712 cm^{-1} and the ground state bleach at 1735 cm^{-1} in the TR-FTIR spectra (Figure 2b), the triplet quantum yield of 4-TU can be estimated based on the Beer–Lambert Law of $A = \epsilon cl$. Here, A is the IR absorption intensity of 4-TU triplet state (A^*) or 4-TU ground state (A^0), which can be obtained from the transient spectra initially after UV excitation at $0.5\ \mu\text{s}$, ϵ is the corresponding IR extinction coefficients of triplet state 4-TU (ϵ^*) or ground state 4-TU (ϵ^0), c is the concentration of 4-TU triplet state (c^*) or excited 4-TU molecules (c^0), l is the path length of the IR cell, which is identical (0.5 mm), and dividing c^* (4-TU triplet state) by c^0 (excited 4-TU molecules) gives the triplet quantum yield of 4-TU. The extinction coefficients of ground state 4-TU (ϵ^0) were obtained from its steady-state FTIR spectra (Figure 2a). By comparing the B3LYP/6-

Table 2. B3LYP/6-311+G(d,p) Calculated IR Frequencies and IR Intensities for Carbonyl Stretching Modes of 4-Thiouracil and Relevant Species in CH_3CN , with the Solvent Effect Simulated by PCM Model, As Well As the Observed IR Frequencies for These Species

	$\nu_{\text{calc}}(C=O)$ cm^{-1}	IR intensity km mol^{-1}	$\nu_{\text{exp}}(C=O)$ cm^{-1}
	1744	1581	1735
4-TU	 1637 (C5=C6)	1063	1623 (C5=C6)
4-TU triplet state	—	1712	1465 1712
(5-4) product	 1686 1749	1514 1544	1685 ^a
(6-4) product	 1694 1745	1867 1520	
(5-4)intermediate —thiol compound	 1690 1741	1421 1571	1681 ^b
(6-4)intermediate —thiol compound	 1691 1734	1508 1419	
uracil	 1732 1699 (C4=O)	662 792	1693 ^c (C4=O)

^{a,b}For the (5-4)/(6-4) intermediates/products, one $C=O$ stretch mode at 1685 or 1681 cm^{-1} was observed in the TR-FTIR spectra, whereas the other $C=O$ stretch mode at higher frequency was buried in the negative band of 4-TU and thus was invisible. ^cThe $C2=O$ band of uracil overlaps with the 4-TU negative band, only the $C4=O$ band was discerned in the TR-FTIR spectra.

311+G(d,p) calculated IR intensities (Table 2), which are proportional to their corresponding extinction coefficients, extinction coefficient for triplet state 4-TU (ϵ^*) can be estimated. This method can be validated by comparing the calculated IR intensities (Table 2) for the two vibrational modes of the ground state 4-TU with the experimental steady-state IR spectra (Figure 2a). The experimental intensity ratio is 0.60 for the $C=C$ stretching mode (1623 cm^{-1}) relative to the $C=O$ stretching mode (1735 cm^{-1}), while the theoretically predicted IR intensities yield a ratio of 0.67 for these two modes. This confirms further that the theoretical IR intensities can be used to estimate unknown IR extinction coefficients.⁴³ By this means, the triplet quantum yield is determined to be ~ 0.9 , which is in excellent agreement with the previously reported value obtained from transient UV–vis absorption measurements,²⁰ demonstrating that TR-FTIR provides an effective alternative method to monitor the triplet states of nucleobases.

Additionally, a small positive band at 1681 cm^{-1} can also be observed in the TR-FTIR spectra (Figure 2b). Unlike the triplet state, which decays fast with a lifetime of $0.23 \pm 0.02\ \mu\text{s}$,

the band at 1681 cm^{-1} decays to the baseline at $2.5\ \mu\text{s}$, with an estimated lifetime of $\sim 2.5\ \mu\text{s}$. This indicates that the weak positive band arises from a transient species other than the triplet 4-TU. Since irradiation of 4-TU at 355 nm can generate (5-4)/(6-4)pyrimidine-pyrimidone cross-linking products⁴⁴ from its triplet state, the 1681 cm^{-1} band may be ascribed to the photo-cross-linking intermediate and its decay corresponds to the formation of pyrimidine–pyrimidone products. According to the calculations (Table 2), the (5-4)/(6-4) intermediates both have vibrational frequencies close to 1681 cm^{-1} . The short-lived intermediates ($2.5\ \mu\text{s}$) are subject to transformation to stable pyrimidine-pyrimidone products. In the steady-state IR absorption difference spectra of N_2 -saturated 4-TU solution recorded after 355 nm irradiation (Figure 2c), together with the strong 4-TU bleaching bands, one positive band at 1685 cm^{-1} is observed prominently, which is characteristic of the formation of the stable product, most likely, the (5-4) or (6-4) pyrimidine-pyrimidone cross-linking products. As shown in Table 2, the predicted vibrational frequencies for the (5-4) or (6-4) intermediates and stable pyrimidine–pyrimidone products are quite close to each other and in agreement with the observed peak position of 1681 or 1685 cm^{-1} in the transient or steady-state IR spectra. The transients at 1681 cm^{-1} in TR-FTIR spectra should correspond to the (5-4)/(6-4) cross-linking intermediates, while the 1685 cm^{-1} band present in the steady-state spectra belongs to the stable products of (5-4)/(6-4) pyrimidine–pyrimidone. Furthermore, the yield of the stable (5-4)/(6-4) product can be obtained from the transient IR absorption spectra (Figure 2b). For the negative band of ground state (1735 cm^{-1}), there is a prominent residual bleach sustained at long delay times (Figure 2b, inset), corresponding to the formation of stable product. Thus, the yield of stable product can be deduced as ~ 0.19 by dividing the amplitude of residual bleach by that of maximum bleach at 1735 cm^{-1} .

The photo-cross-linking reaction to form (5-4) or (6-4) pyrimidine-pyrimidone products was suggested to begin with the [2 + 2] addition of the $\text{C}=\text{S}$ double bond of 4-TU to the $5,6\text{-C}=\text{C}$ of another pyrimidine such as another 4-TU. It initially produces the four-membered ring intermediate, thietane.⁴⁴ The thietane would be expected to be very unstable and open the ring rapidly to form the next intermediate, a thiol compound, with its structure shown in Table 2. The following elimination of hydrogen sulfide from the thiol intermediate would lead to the (5-4) or (6-4) products. In our TR-FTIR spectra, the proposed thiol intermediates of (5-4) or (6-4) photo cross-linking reaction has been observed, thus allowing further justification for the proposed (5-4) or (6-4) photo-cross-linking mechanism. The lowest triplet state (T_1) of 4-TU was suggested to be a π,π^* state with a minor energy gap to the second triplet state (T_2), which has a n,π^* character. Thus, the T_1 state can be mixed with some n,π^* character, making the $\text{C}=\text{S}$ bond liable to the (5-4) or (6-4) photo-cross-linking reactions.

3.3. Aerobic Conditions: Triplet and Its Photochemistry Characterization with TR-FTIR Absorption Spectroscopy. Upon UVA excitation, the high triplet quantum yield of 4-TU can further generate singlet oxygen $^1\text{O}_2$ through photosensitization in aerobic conditions, resulting in complex photochemistry relevant to singlet oxygen. Figure 3a displays the TR-FTIR spectra of 4-TU in O_2 -saturated solution after the nanosecond 355 nm laser irradiation. Initially after UV excitation at $0.5\ \mu\text{s}$, the two ground state bleaching bands are observed together with the triplet positive band at

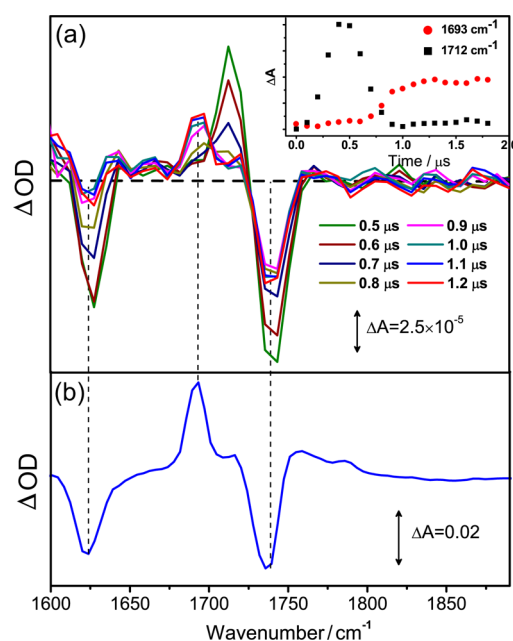


Figure 3. (a) Infrared transient absorption (TR-FTIR) spectra of 1.0 mM solution of 4-TU in acetonitrile saturated with O_2 following 355 nm laser irradiation. The spectra were collected with a resolution of 16 cm^{-1} . (b) Steady-state IR difference spectrum of 4-TU (1.0 mM) in acetonitrile saturated with O_2 after 1 min of 355 nm laser irradiation. The spectrum was collected with a resolution of 8 cm^{-1} .

1712 cm^{-1} . Since O_2 can efficiently quench triplet state, the signal intensity here is weak and decays more rapidly than in N_2 -saturated solution, with the lifetime shortened to $0.17 \pm 0.02\ \mu\text{s}$. Considering the saturated concentration of oxygen in acetonitrile (1.9 mM), the quenching rate constant of triplet 4-TU by oxygen is $\sim 3.1 \times 10^9\text{ M}^{-1}\text{ s}^{-1}$, consistent with the reported value of $4 \times 10^9\text{ M}^{-1}\text{ s}^{-1}$.¹⁸ Meanwhile, a photoproduct species is observed in the TR-FTIR spectra with a characteristic absorption band at $\sim 1693\text{ cm}^{-1}$. This band decays slowly at several hundreds of μs in the TR-FTIR spectra and is also clearly observed in the steady-state FTIR difference spectra (Figure 3b), indicating that it belongs to a stable species. According to its spectral position, this band should be ascribed to the $\text{C4}=\text{O}$ carbonyl stretching mode of uracil,⁴⁵ one of the possible photoproducts after UV irradiation of 4-TU.¹⁸ The calculations predict vibrational frequencies for $\text{C4}=\text{O}$ of uracil at 1699 cm^{-1} and for $\text{C2}=\text{O}$ at 1732 cm^{-1} , as shown in Table 2. Because the $\text{C2}=\text{O}$ band overlaps with one of the 4-TU negative band, only the $\text{C4}=\text{O}$ band at 1693 cm^{-1} for the product uracil is observed in the TR-FTIR spectra.

It shows here in the TR-FTIR spectra that quenching of 4-TU triplet state by O_2 led to the formation of stable product uracil. Two types of processes were suggested to result in the conversion of 4-TU to uracil under UV excitation.¹⁸ However, it is not clear whether the formation of uracil is due to direct photoreaction of the 4-TU triplet state with oxygen or whether it predominantly results from oxidation of ground state 4-TU by singlet oxygen $^1\text{O}_2$, which is produced in high yield by energy transfer from 4-TU triplet state.²⁸ This problem can be resolved here from our TR-FTIR measurements. The kinetics of triplet state decay and uracil formation are displayed in Figure 3a inset. It can be clearly seen that the formation of uracil (1693 cm^{-1}) lags behind the decay of 4-TU triplet state (1712 cm^{-1}). Only when the triplet signal decays completely to

the baseline, the uracil band (1693 cm^{-1}) starts to grow up. This indicates that uracil is not directly formed from the triplet reaction, but rather through another reactive species generated after the complete quenching of triplet. Since the quenching of triplet corresponds to the formation of singlet oxygen in aerobic conditions, the product uracil should arise from the reaction of singlet oxygen with 4-TU. It will be discussed in section 3.5 that the calculated potential energy profiles for $^1\text{O}_2$ reacting with 4-TU also supports this mechanism.

For the identified uracil (U) formation pathway from $^1\text{O}_2$ reacting with 4-TU, the product yields can be further quantified. TR-FTIR absorption spectra measure simultaneously the depletion of reactant molecules with the formation of photoproducts. Thus, adopting the positive bands of photoproducts (1693 cm^{-1}) with maximum intensity and the negative band of reactants (1735 cm^{-1}) with plateau intensity, both the amount of photoproduct formed and reactant consumed can be quantified by normalizing the peak area of the IR absorption band with the absorption coefficient.⁴³ Furthermore, dividing the amount of photoproduct formation by reactant consumption gives the absolute yield for the photoproduct, which is ~ 0.2 for the uracil formation pathway.

3.4. Aerobic Conditions: Photoproduct Formation Characterized by Fluorescence Spectroscopy. In addition to the stable product uracil observed from TR-FTIR, another product of $4\text{-TU} + ^1\text{O}_2$ can be also identified from fluorescence spectra. Figure 4a displays the fluorescence spectrum and excitation spectrum of 4-TU after 1.5 min of 355 nm irradiation, in O_2 -saturated phosphate buffer solution (pH = 7.0). A fluorescent product with an emission peak at $\sim 390\text{ nm}$ is observed. The excitation spectrum of the fluorescent product shows an absorption peak at $\sim 310\text{ nm}$. The oxidation of 4-TU by the strong oxidant KMnO_4 is known to produce the fully oxidized product uracil-6-sulfonate (U^{SO_3}),⁴⁶ with the excitation and emission spectra (Figure 4b) resembling those recorded for the 4-TU under $^1\text{O}_2$ oxidation (Figure 4a). This suggests U^{SO_3} to be a product for the reaction of 4-TU with $^1\text{O}_2$. This result can find an analogue in another similar thionucleobase 6-thioguanine, where the UVA photosensitization led to $^1\text{O}_2$ and its subsequent reaction with 6-thioguanine formed the fully oxidized fluorescent product guanine-6-sulfonate (G^{SO_3}).^{29,30} The assignment of the $\sim 390\text{ nm}$ fluorescent product to U^{SO_3} can be further supported by our TD-DFT calculations. For U^{SO_3} , the absorption wavelength (298 nm) calculated at the TD-B3LYP/6-311+G(d,p) level fits with the experimental value of $\sim 310\text{ nm}$ more closely, compared with the result (281 nm) obtained at the TD-WB97XD/6-311+G(d,p) level. On the other hand, the TD-WB97XD/6-311+G(d,p) level of theory yields better result (406 nm) in calculating the fluorescence wavelength than that (487 nm) obtained by TD-B3LYP/6-311+G(d,p). This is probably caused by the inclusion of empirical dispersion in the WB97XD functional, which can well optimize the excited state geometry. As shown in Figure 4c,d, the nonplanar feature of the excited state geometry (distortion of the pyrimidine ring along the N1...C4 axis) is well exhibited by the TD-WB97XD/6-311+G(d,p) calculations, whereas the TD-B3LYP/6-311+G(d,p) calculations do not reflect this structural change (excited state geometry is still planar as that in ground state).

3.5. Theoretical Characterization for the Photochemical Reaction of 4-TU with $^1\text{O}_2$. By means of TR-FTIR and fluorescence spectroscopy, it is shown that the UVA (355 nm) photosensitization of 4-TU leads to $^1\text{O}_2$, which then

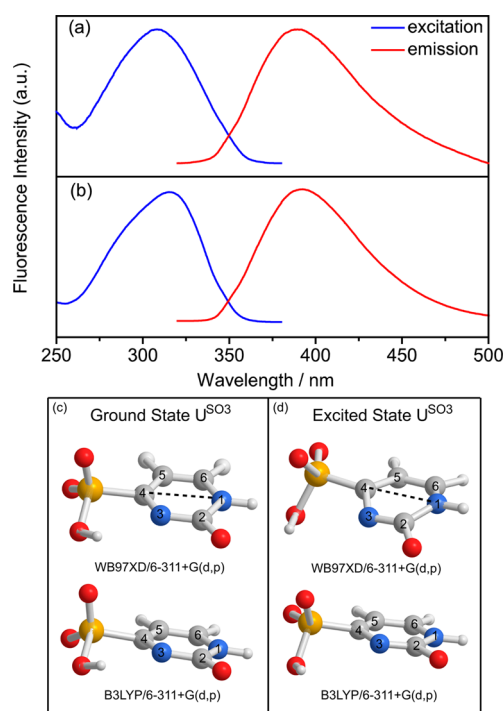


Figure 4. (a) The excitation (blue line) and emission (red line) spectra for the product of 4-TU in phosphate buffer (pH = 7.0) under O_2 -saturated conditions after 1.5 min of 355 nm laser irradiation. (b) The excitation (blue line) and emission (red line) spectra of U^{SO_3} generated by complete oxidation of 4-TU by KMnO_4 . Excitation wavelength for the emission spectrum was 310 nm and the monitoring wavelength for the excitation spectrum was 392 nm . (c) The ground state geometries and (d) excited state geometries of U^{SO_3} optimized respectively at the TD-B3LYP/6-311+G(d,p) and TD-WB97XD/6-311+G(d,p) level. Carbon, oxygen, nitrogen, sulfur, and hydrogen atoms are denoted with gray, red, blue, yellow, and white balls, respectively.

reacts readily with 4-TU to form two products, U and U^{SO_3} . To explore the reaction mechanism, we performed theoretical calculations at the B3LYP/6-311+G(d,p) level with the solvent effect simulated by PCM. The possibility of triplet 4-TU reacting with ground state O_2 was also explored at the B3LYP/6-311+G(d,p) level, but it is found that no bonds can be formed between triplet state 4-TU and ground state oxygen, indicating that the reaction cannot take place between triplet state 4-TU and ground state oxygen. In contrast, as will be discussed below, calculation results indicate that the reaction of 4-TU with singlet oxygen proceeds readily. Together with our TR-FTIR results discussed above, it is demonstrated clearly that the photoreaction of 4-TU under oxygen-saturation conditions is mainly due to the oxidation of ground state 4-TU by the photosensitization formed singlet oxygen.

Figures 5 and 6 display the potential energy profiles obtained for the reaction of 4-TU with $^1\text{O}_2$. Cartesian coordinates for the optimized structures are listed in Table S1 and S2. Although singlet oxygen ($^1\text{O}_2$) is an excited species, the reaction of $^1\text{O}_2$ with 4-TU takes place on the ground state with the spin multiplicity of 1 and only closed-shell stationary points are involved, which can be calculated by the B3LYP/6-311+G(d,p) level of theory. For the first stationary point involving the initial reactant complex of $4\text{-TU}\cdots^1\text{O}_2$ (IM1) before bonding occurs, $^1\text{O}_2$ was treated as a ground state entity under approximation. As shown in Figure 5, the reactant 4-TU and $^1\text{O}_2$ forms a

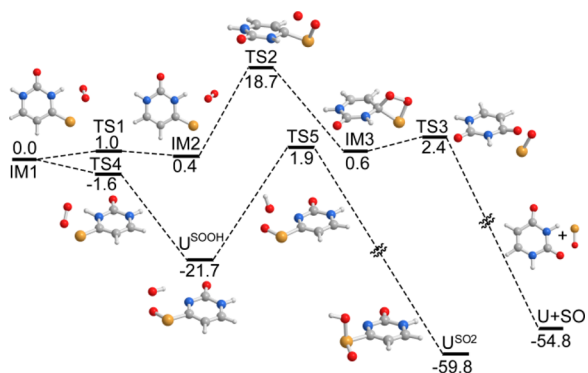


Figure 5. Potential energy profiles for the 4-TU reaction with ${}^1\text{O}_2$ toward the formation of the partially oxidized product U^{SO_2} and the minor product U. The energies (in kcal mol^{-1}) are obtained at the B3LYP/6-311+G(d,p) level with the solvent effect simulated by PCM. All energies given are relative to the reactant complex IM1 (4-TU \cdots ${}^1\text{O}_2$). Carbon, oxygen, nitrogen, sulfur, and hydrogen atoms are denoted with gray, red, blue, yellow, and white balls, respectively.

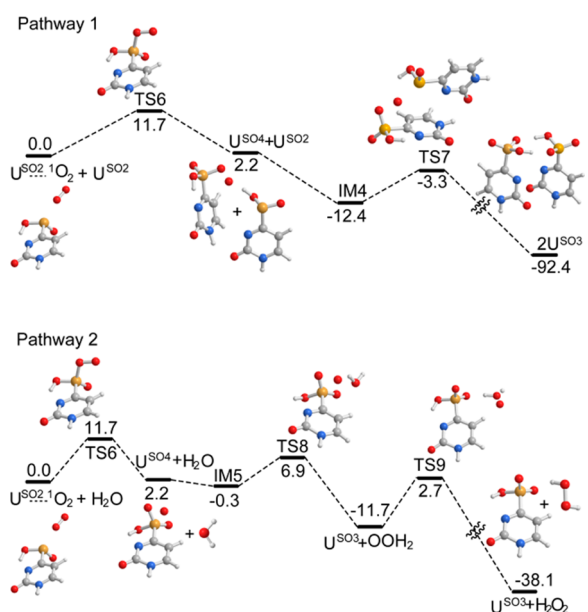


Figure 6. Potential energy profiles for the formation of the fully oxidized product U^{SO_3} , preceded by the intermediate of U^{SO_2} . The energies (in kcal mol^{-1}) are obtained at the B3LYP/6-311+G(d,p) level with the solvent effect simulated by PCM. All energies given are relative to the reactant complexes of different pathways. Carbon, oxygen, nitrogen, sulfur, and hydrogen atoms are denoted with gray, red, blue, yellow, and white balls, respectively.

complex 4-TU \cdots ${}^1\text{O}_2$ (IM1) via a weak hydrogen bond initially, which is followed by the ${}^1\text{O}_2$ bonding with the sulfur atom and the simultaneous hydrogen abstraction by the dangling oxygen atom from the neighboring NH moiety, leading to the formation of the peroxy intermediate U^{SOOH} with an S–O–O–H geometry. The cleavage of the weak O–O bond of U^{SOOH} and the bonding of the departing OH to sulfur atom leads to U^{SO_2} (via TSS). Basically, the formation of U^{SO_2} occurs easily at room temperature because the rate-limiting step (from U^{SOOH} to TSS) has a low barrier of only $1.9 \text{ kcal mol}^{-1}$ and TS4 is lower in energy than the reactant complex IM1. In addition, U^{SO_2} lies $59.8 \text{ kcal mol}^{-1}$ below the reactant complex, indicating its stability.

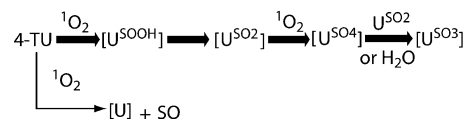
In competition with U^{SO_2} formation, another pathway leading to stable product U can be located. Starting from the complex 4-TU \cdots ${}^1\text{O}_2$ (IM2), O–O bond of ${}^1\text{O}_2$ can undergo a [2 + 2] cycloaddition to the C=S bond of 4-TU, forming a four-membered (OCSO) ring intermediate IM3. The C=S bond in IM3 is thus weakened, and the cleavage of the C=S bond leads to product uracil (U). The pathway forming U is rate-limited by a barrier of $18.7 \text{ kcal mol}^{-1}$ for the cycloaddition step, which is much higher than the U^{SO_2} formation and thus indicates a less favorable formation of U in the total reaction. This result explains our experimental observation of U as a minor product with a yield of ~ 0.2 .

Following the facile formation of U^{SO_2} , further oxidation to U^{SO_3} can still occur, due to the unsaturated bonding valence of sulfur atom and the high reactivity of ${}^1\text{O}_2$. As a relatively stable primary product, U^{SO_2} can serve as the reactant and can be involved in subsequent oxidation reaction steps. Two pathways leading to the fully oxidized product U^{SO_3} have been located, which are all preceded by the formation of U^{SO_2} (Figure 6). In pathway 1, addition of singlet oxygen to U^{SO_2} leads to another peroxy intermediate U^{SO_4} , overcoming a barrier of $11.7 \text{ kcal mol}^{-1}$. The intermediate U^{SO_4} is quite reactive. The oxygen atom in U^{SO_4} can be easily abstracted by another U^{SO_2} , forming two U^{SO_3} molecules via a barrier of $9.1 \text{ kcal mol}^{-1}$ (from IM4 to TS7). U^{SO_3} is the most stable final product that is refractory to further oxidation, because it falls around the global minimum of the potential energy surface with energy of $92.4 \text{ kcal mol}^{-1}$ below the reactant complex of $\text{U}^{\text{SO}_2}\cdots{}^1\text{O}_2$.

Once the peroxy intermediate U^{SO_4} is formed as in pathway 1, another route is open for the formation of U^{SO_3} , through the participation of water molecules. H_2O can form a hydrogen-bonded complex (IM5) with U^{SO_4} , through which the oxygen atom in U^{SO_4} is abstracted by H_2O via TS8, yielding the stable product U^{SO_3} and H_2O_2 . This constitutes pathway 2. In pathway 2, only low barriers of $11.7 \text{ kcal mol}^{-1}$ (for the U^{SO_4} formation step) and $6.9 \text{ kcal mol}^{-1}$ (from IM5 to TS8) are involved. Considering the use of aqueous solution as reaction medium, the ubiquitous presence of water molecules may greatly facilitate this pathway.

Overall, the energetically accessible pathways for the reaction of 4-TU with ${}^1\text{O}_2$ can be summarized in Scheme 2. According

Scheme 2. Elucidated Reaction Mechanisms for 4-TU with ${}^1\text{O}_2$ ^a



^aThe more favorable reaction pathways are shown with bold arrows.

to the calculated potential energy profiles in Figure 5, a predominant formation of U^{SO_2} over U formation is expected. Once U^{SO_2} is formed, the subsequent oxidation to U^{SO_3} takes place readily. So, according to the calculated pathways, the successive formation of U^{SO_2} and U^{SO_3} is expected to predominate that of the product U. This is consistent with our TR-FTIR result that the product yield of U is low (0.2). Altogether, the results obtained here for 4-TU is similar to previous results for another thionucleobase of 6-thioguanine.^{30,47,48}

4. CONCLUSIONS

In summary, from dynamics and mechanistic point of views, the joint TR-FTIR spectroscopy and DFT studies performed here provide a further understanding of the unique photophysical and photochemical properties of the thionucleobase, 4-TU. It is shown that 4-TU absorbs UVA and results in the triplet formation with a high quantum yield (0.9). Under N₂-saturated anaerobic conditions, the reactive triplet undergoes mainly cross-linking with ground state 4-TU, leading to the (5-4)/(6-4) pyrimidine-pyrimidone product. In the presence of O₂ under aerobic conditions, the triplet 4-TU acts as an energy donor to produce singlet oxygen ¹O₂ by triplet-triplet energy transfer. The highly reactive oxygen species ¹O₂ then reacts readily with 4-TU, leading to the products of uracil (U) with a yield of 0.2 and uracil-6-sulfonate (U^{SO3}) that is fluorescent at ~390 nm. These product formation pathways and product distribution can be well rationalized by the joint B3LYP/6-311+G(d,p) calculations. The calculations reveal the mechanism of U^{SO3} formation through the successive peroxy intermediate pathway of U^{SOOH} → U^{SO2} → U^{SO4} → U^{SO3} and the U formation mechanism through ¹O₂ addition to C=S bond of 4-TU. Lower barriers are involved for U^{SO3} formation compared to those for U formation. The overall reaction is suggested in the potential energy profiles to be energetically favorable, explaining the high reactivity of ¹O₂ oxidizing 4-TU.

These results indicate that 4-TU can act as a strong UVA photosensitizer, providing a source of the reactive oxygen species of ¹O₂, which has profound impact on photo cross-linking, photodamage, as well as photodynamic therapy studies. In particular, considering that 4-TU is usually adopted as a site-specific photoprobe by its triplet photo cross-linking reactions with other nucleic acids or proteins, our results suggest that the photosensitization of 4-TU to generate ¹O₂ under aerobic conditions and the ensuing highly reactive ¹O₂ reactions can compete strongly with the photo-cross-linking, thus making the photochemistry rather complex in these studies. For applications of 4-TU as photoprobe to elucidate RNA structure, to unravel nucleic acid-nucleic acid contacts within complex assemblies, and so on, the influence of the 4-TU as reactive precursors of ¹O₂ and the induced oxidation reactions should also be carefully considered.

■ ASSOCIATED CONTENT

Supporting Information

Cartesian coordinate for optimized structures along potential energy profiles of Figures 5 and 6. This material is available free of charge via the Internet at <http://pubs.acs.org>.

■ AUTHOR INFORMATION

Corresponding Author

*E-mail: hongmei@iccas.ac.cn.

Notes

The authors declare no competing financial interest.

■ ACKNOWLEDGMENTS

This work was financially supported by the National Natural Science Foundation of China (Grant Nos. 21073201, 21333012) and the National Basic Research Program of China (2013CB834602).

■ REFERENCES

- (1) Morrison, H. *Bioorganic Photochemistry: Photochemistry and the nucleic acids*; Wiley: New York, 1990; Vol. 1.
- (2) Merchán, M.; González-Luque, R.; Climent, T.; Serrano-Andrés, L.; Rodríguez, E.; Reguero, M.; Peláez, D. Unified Model for the Ultrafast Decay of Pyrimidine Nucleobases. *J. Phys. Chem. B* **2006**, *110*, 26471–26476.
- (3) Crespo-Hernández, C. E.; Cohen, B.; Hare, P. M.; Kohler, B. Ultrafast Excited-State Dynamics in Nucleic Acids. *Chem. Rev. (Washington, DC, U. S.)* **2004**, *104*, 1977–2020.
- (4) Perun, S.; Sobolewski, A. L.; Domcke, W. Conical Intersections in Thymine. *J. Phys. Chem. A* **2006**, *110*, 13238–13244.
- (5) Matsika, S. Radiationless Decay of Excited States of Uracil through Conical Intersections. *J. Phys. Chem. A* **2004**, *108*, 7584–7590.
- (6) Middleton, C. T.; de La Harpe, K.; Su, C.; Law, Y. K.; Crespo-Hernández, C. E.; Kohler, B. DNA Excited-State Dynamics: From Single Bases to the Double Helix. *Annu. Rev. Phys. Chem.* **2009**, *60*, 217–239.
- (7) Keane, P. M.; Wojdyla, M.; Doorley, G. W.; Watson, G. W.; Clark, I. P.; Greetham, G. M.; Parker, A. W.; Towrie, M.; Kelly, J. M.; Quinn, S. J. A Comparative Picosecond Transient Infrared Study of 1-Methylcytosine and 5'-dCMP That Sheds Further Light on the Excited States of Cytosine Derivatives. *J. Am. Chem. Soc.* **2011**, *133*, 4212–4215.
- (8) Pecourt, J.-M. L.; Peon, J.; Kohler, B. DNA Excited-State Dynamics: Ultrafast Internal Conversion and Vibrational Cooling in a Series of Nucleosides. *J. Am. Chem. Soc.* **2001**, *123*, 10370–10378.
- (9) Malone, R. J.; Miller, A. M.; Kohler, B. Singlet Excited-state Lifetimes of Cytosine Derivatives Measured by Femtosecond Transient Absorption. *Photochem. Photobiol.* **2003**, *77*, 158–164.
- (10) Pecourt, J.-M. L.; Peon, J.; Kohler, B. Ultrafast Internal Conversion of Electronically Excited RNA and DNA Nucleosides in Water. *J. Am. Chem. Soc.* **2000**, *122*, 9348–9349.
- (11) Gustavsson, T.; Sarkar, N.; Lazzarotto, E.; Markovitsi, D.; Improta, R. Singlet Excited State Dynamics of Uracil and Thymine Derivatives: A Femtosecond Fluorescence Upconversion Study in Acetonitrile. *Chem. Phys. Lett.* **2006**, *429*, 551–557.
- (12) Pancur, T.; Schwalb, N. K.; Renth, F.; Temps, F. Femtosecond Fluorescence Up-Conversion Spectroscopy of Adenine and Adenosine: Experimental Evidence for the ππ* State? *Chem. Phys.* **2005**, *313*, 199–212.
- (13) Peon, J.; Zewail, A. H. DNA/RNA Nucleotides and Nucleosides: Direct Measurement of Excited-state Lifetimes by Femtosecond Fluorescence Up-Conversion. *Chem. Phys. Lett.* **2001**, *348*, 255–262.
- (14) Towrie, M.; Doorley, G. W.; George, M. W.; Parker, A. W.; Quinn, S. J.; Kelly, J. M. ps-TRIR Covers all the Bases - Recent Advances in the Use of Transient IR for the Detection of Short-Lived Species in Nucleic Acids. *Analyst* **2009**, *134*, 1265–1273.
- (15) Lipsett, M. N. The Isolation of 4-Thiouridylic Acid from the Soluble Ribonucleic Acid of *Escherichia coli*. *J. Biol. Chem.* **1965**, *240*, 3975–3978.
- (16) Zachau, H. G. Transfer Ribonucleic Acids. *Angew. Chem., Int. Ed. Engl.* **1969**, *8*, 711–727.
- (17) Pleiss, M. G.; Cerutti, P. A. Phototransformation of 4-Thiouridine in *Escherichia coli* Valine Transfer Ribonucleic Acid to Uridine, Cytidine, and N⁴-Methylcytidine. *Biochemistry* **1971**, *10*, 3093–3099.
- (18) Favre, A.; Saintome, C.; Fourrey, J. L.; Clivio, P.; Laugaa, P. Thionucleobases as Intrinsic Photoaffinity Probes of Nucleic Acid Structure and Nucleic Acid Protein Interactions. *J. Photochem. Photobiol., B* **1998**, *42*, 109–124.
- (19) Salet, C.; Bensasson, R. V.; Favre, A. Studies on the Triplet Excited State of 4-Thiouridine. *Photochem. Photobiol.* **1983**, *38*, 521–525.
- (20) Milder, S. J.; Kliger, D. S. Spectroscopy and Photochemistry of Thiouracils: Implications for the Mechanism of Photocrosslinking in tRNA. *J. Am. Chem. Soc.* **1985**, *107*, 7365–7373.

- (21) Padró, T.; van den Hoogen, C. M.; Emeis, J. J. Experimental Hypothyroidism Increases Plasminogen Activator Inhibitor Activity in Rat Plasma. *Blood Coagul. Fibrinolysis* **1993**, *4*, 797–800.
- (22) Peebles, E. D.; Miller, E. H.; Boyle, C. R.; Brake, J. D.; Latour, M. A. Effects of Dietary Thiouracil on Thyroid Activity, Egg Production, and Eggshell Quality in Commercial Layers. *Poult. Sci.* **1994**, *73*, 1829–1837.
- (23) Aarbakke, J.; JankaSchaub, G.; Elion, G. B. Thiopurine Biology and Pharmacology. *Trends Pharmacol. Sci.* **1997**, *18*, 3–7.
- (24) Shalitin, N.; Feitelson, J. 4-Thiouridine, a Built-in Probe for Structural Changes in Transfer RNA. *Biochemistry* **1976**, *15*, 2092–2097.
- (25) Wang, Z.; Rana, T. M. RNA Conformation in the Tat–TAR Complex Determined by Site-Specific Photo-Cross-Linking. *Biochemistry* **1996**, *35*, 6491–6499.
- (26) Meisenheimer, K. M.; Koch, T. H. Photocross-Linking of Nucleic Acids to Associated Proteins. *Crit. Rev. Biochem. Mol. Biol.* **1997**, *32*, 101–140.
- (27) Shukla, M. K.; Leszczynski, J. Electronic Transitions of Thiouracils in the Gas Phase and in Solutions: Time-Dependent Density Functional Theory (TD-DFT) Study. *J. Phys. Chem. A* **2004**, *108*, 10367–10375.
- (28) Heihoff, K.; Redmond, R. W.; Braslavsky, S. E.; Rougee, M.; Salet, C.; Favre, A.; Bensasson, R. V. Quantum Yields of Triplet and $O_2(^1\Delta_g)$ Formation of 4-Thiouridine in Water and Acetonitrile. *Photochem. Photobiol.* **1990**, *51*, 635–641.
- (29) Zhang, Y. Z.; Zhu, X. C.; Smith, J.; Haygood, M. T.; Gao, R. M. Direct Observation and Quantitative Characterization of Singlet Oxygen in Aqueous Solution upon UVA Excitation of 6-Thioguanines. *J. Phys. Chem. B* **2011**, *115*, 1889–1894.
- (30) Ren, X. L.; Li, F.; Jeffs, G.; Zhang, X. H.; Xu, Y. Z.; Karran, P. Guanine Sulphinic Acid is a Major Stable Product of Photochemical Oxidation of DNA 6-Thioguanine by UVA Irradiation. *Nucleic Acids Res.* **2010**, *38*, 1832–1840.
- (31) Uhmann, W.; Becker, A.; Taran, C.; Siebert, F. Time-Resolved FT-IR Absorption Spectroscopy Using a Step-Scan Interferometer. *Appl. Spectrosc.* **1991**, *45*, 390–397.
- (32) Drapcho, D. L.; Curbelo, R.; Jiang, E. Y.; Crocombe, R. A.; McCarthy, W. J. Digital Signal Processing for Step-Scan Fourier Transform Infrared Photoacoustic Spectroscopy. *Appl. Spectrosc.* **1997**, *51*, 453–460.
- (33) Lee, C. T.; Yang, W. T.; Parr, R. G. Development of the Colle–Salvetti Correlation-Energy Formula into a Functional of the Electron-Density. *Phys. Rev. B* **1988**, *37*, 785–789.
- (34) Becke, A. D. Density-Functional Thermochemistry 0.3. The Role of Exact Exchange. *J. Chem. Phys.* **1993**, *98*, 5648–5652.
- (35) Gonzalez, C.; Schlegel, H. B. Reaction Path Following in Mass-Weighted Internal Coordinates. *J. Phys. Chem.* **1990**, *94*, 5523–5527.
- (36) Mennucci, B.; Tomasi, J. Continuum Solvation Models: A New Approach to the Problem of Solute's Charge Distribution and Cavity Boundaries. *J. Chem. Phys.* **1997**, *106*, 5151–5158.
- (37) Chai, J.-D.; Head-Gordon, M. Long-Range Corrected Hybrid Density Functionals with Damped Atom–Atom Dispersion Corrections. *Phys. Chem. Chem. Phys.* **2008**, *10*, 6615–6620.
- (38) Frisch, M. J.; Trucks, G. W.; Schlegel, H. B.; Scuseria, G. E.; Robb, M. A.; Cheeseman, J. R.; Scalmani, G.; Barone, V.; Mennucci, B.; Petersson, G. A.; et al. *Gaussian 09*, revision B.01; Gaussian, Inc.: Wallingford, CT, 2009.
- (39) Taras-Goslinska, K.; Wenska, G.; Skalski, B.; Maciejewski, A.; Burdzinski, G.; Karolczak, J. Spectral and Photophysical Properties of the Lowest Excited Triplet State of 4-Thiouridine and Its 5-Halogeno Derivatives. *J. Photochem. Photobiol., A* **2004**, *168*, 227–233.
- (40) Psoda, A.; Kazimier, Z.; Shugar, D. Structure and Tautomerism of the Neutral and Monoanionic Forms of 4-Thiouracil Derivatives. *J. Am. Chem. Soc.* **1974**, *96*, 6832–6839.
- (41) Rostkowska, H.; Szczepaniak, K.; Nowak, M. J.; Leszczynski, J.; KuBulat, K.; Person, W. B. Thiouracils. 2. Tautomerism and Infrared Spectra of Thiouracils. Matrix-Isolation and Ab Initio Studies. *J. Am. Chem. Soc.* **1990**, *112*, 2147–2160.
- (42) Taras-Goslinska, K.; Wenska, G.; Skalski, B.; Maciejewski, A.; Burdzinski, G.; Karolczak, J. Intra- and Intermolecular Electronic Relaxation of the Second Excited Singlet and the Lowest Excited Triplet States of 1,3-Dimethyl-4-thiouracil in Solution. *Photochem. Photobiol.* **2002**, *75*, 448–456.
- (43) Wu, W.; Liu, K.; Yang, C.; Zhao, H.; Wang, H.; Yu, Y.; Su, H. Reaction Mechanisms of a Photo-Induced [1,3] Sigmatropic Rearrangement via a Nonadiabatic Pathway. *J. Phys. Chem. A* **2009**, *113*, 13892–13900.
- (44) Bergstrom, D. E.; Leonard, N. J. Photoreaction of 4-Thiouracil with Cytosine. Relation to Photoreactions in *Escherichia coli* Transfer Ribonucleic Acids. *Biochemistry* **1972**, *11*, 1–9.
- (45) Yang, C. F.; Yu, Y. Q.; Liu, K. H.; Song, D.; Wu, L. D.; Su, H. M. 2 + 2 Photocycloaddition Reaction Dynamics of Triplet Pyrimidines. *J. Phys. Chem. A* **2011**, *115*, 5335–5345.
- (46) Hayatsu, H.; Yano, M. Permanganate Oxidation of 4-Thiouracil Derivatives. Isolation and Properties of 1-Substituted-2-pyrimidone-4-sulfonates. *Tetrahedron Lett.* **1969**, *10*, 755–758.
- (47) O'Donovan, P.; Perrett, C. M.; Zhang, X. H.; Montaner, B.; Xu, Y. Z.; Harwood, C. A.; McGregor, J. M.; Walker, S. L.; Hanaoka, F.; Karran, P. Azathioprine and UVA Light Generate Mutagenic Oxidative DNA Damage. *Science* **2005**, *309*, 1871–1874.
- (48) Zou, X. R.; Zhao, H. M.; Yu, Y. Q.; Su, H. M. Formation of Guanine-6-sulfonate from 6-Thioguanine and Singlet Oxygen: A Combined Theoretical and Experimental Study. *J. Am. Chem. Soc.* **2013**, *135*, 4509–4515.